SPECIAL TOPICS — Acoustics

Spatial correlation of the high intensity zone in deep-water acoustic field*

Jun Li(李鋆)[1,2], Zheng-Lin Li(李整林)[1,3,†], and Yun Ren(任云)[1]

[1] State Key Laboratory of Acoustics, Institute of Acoustics, Chinese Academy of Sciences, Beijing 100190, China

[2] University of Chinese Academy of Sciences, Beijing 100190, China

[3] Haikou Laboratory of Acoustics, Institute of Acoustics, Chinese Academy of Sciences, Haikou 570105, China

(Received 7 June 2016; revised manuscript received 11 August 2016; published online 25 October 2016)

The spatial correlations of acoustic field have important implications for underwater target detection and other applications in deep water. In this paper, the spatial correlations of the high intensity zone in the deep-water acoustic field are investigated by using the experimental data obtained in the South China Sea. The experimental results show that the structures of the spatial correlation coefficient at different ranges and depths are similar to the transmission loss structure in deep water. The main reason for this phenomenon is analyzed by combining the normal mode theory with the ray theory. It is shown that the received signals in the high intensity zone mainly include one or two main pulses which are contributed by the interference of a group of waterborne modes with similar phases. The horizontal-longitudinal correlations at the same receiver depth but in different high intensity zones are analyzed. At some positions, more pulses are received in the arrival structure of the signal due to bottom reflection and the horizontal-longitudinal correlation coefficient decreases accordingly. The multi-path arrival structure of receiving signal becomes more complex with increasing receiver depth.

Keywords: spatial correlations, deep water, high intensity zone, normal mode

PACS: 43.30.Bp, 43.30.Re, 43.30.Dr **DOI:** 10.1088/1674-1056/25/12/124310

1. Introduction

The spatial correlation of an acoustic field is an important characteristic for describing sound propagation in the ocean. The spatial correlation radius of the acoustic field has considerable influence on the performance of the hydrophone array beamforming spatial gain. Recently, the vertical correlation has been studied extensively and applied to practical underwater acoustic signal processing.[1,2] However, there are relatively few experimental results of the horizontal correlation because it is difficult to deploy a large-scale horizontal array. The research on the horizontal correlation is the physical foundation of large scale horizontal receiving sonar array applications in the future. With the development of the signal processing technique (such as passive synthetic aperture and time-reversal retrofocusing of horizontal linear array) of the large scale receiving sonar array,[3,4] and in order to improve the angular resolution of sonar and enhance the signal gain, studying the horizontal correlations of an acoustic field and its variability with environmental changes becomes more and more important.

The convergence zone in deep water was first found in the 1950s. Hale[5] described that the convergence zone was the result of the sound wave emitted from a shallow source. The sound wave was refracted and reversed from the surface at a range of about 30–35 miles (1 miles = 1.609344 km) and formed a several-kilometer width high intensity zone.[5] Generally, the source and receiver are near the surface in the actual detection of an underwater acoustic signal, therefore, we can use convergence zones of the SOFAR channel for the long distance detection. As is well known, the characteristics of the high intensity zone inside deep water which is made up of caustics are similar to those of the convergence zone near the surface. In this paper, the object to be investigated includes all high-intensity zones in deep water.

Recently, some work on the spatial correlations in deep water has been done. Urick and Lund,[6] and Urick[7] investigated the vertical coherence of underwater sound in a convergence zone by using explosive signals and ray theory in the 1960s. They calculated that the correlation coefficient equaled nearly unity when hydrophones were in the convergence half-zones, and showed only a slow falloff with increasing separation. In between zones, where bottom-reflected paths occur, the correlation coefficient was much smaller and fell off faster with increasing separation. In the 1980s, Zhang theoretically analyzed the acoustic field of the turning-point convergence-zone by normal mode theory and ray theory,[8,9] respectively. He came to the conclusion that the acoustic field of the turning-point convergence-zone is the superposition of a

*Project supported by the National Natural Science Foundation of China (Grant Nos. 11434012 and 41561144006).

†Corresponding author. E-mail: lzhl@mail.ioa.ac.cn

© 2016 Chinese Physical Society and IOP Publishing Ltd

great number of in-phase normal modes and the received signals in turning-point convergence-zones have the same waveform as the emitted signal or its Hilbert transform for high-frequency and narrow-band signals. Reference [10] presented the results of deep-water acoustic coherence at long ranges in summer and winter conditions. Colosi and Tarum simulated the horizontal coherence by using both the quadratic transport theory and quadratic adiabatic based on a deep-water Philippine Sea environment.[11] They obtained that the coherence length at the 500 km range is about 1900 m, of which the range scaling is precisely $R^{-1/2}$ and the frequency scaling is close to $f^{-1.12}$. Reference [12] indicated that the horizontal-longitudinal correlation coefficients in a convergence zone are high, and the correlation radius is consistent with the convergence zone width, but the correlation radius in the shadow zone is much shorter. Reference [4] analyzed the influence of the horizontal correlation radius on passive synthetic aperture (PASA) performance in a deep-water acoustic field. It came to the conclusion that because the horizontal correlation radius of the sound field is short in the shadow zone, the performance of PASA is limited to near the conventional physical aperture array. In contrast, the performance of PASA is remarkably better than the conventional physical aperture array in the convergence zone of the ocean waveguide since the horizontal correlation radius is large. However, the problem of the spatial correlations between the high intensity zones at different ranges and depths in the deep water acoustic field is still not well understood.

In this paper, firstly, we present the experimental result about the spatial correlations of the high intensity zone in the deep water acoustic field by using the experimental data obtained in the South China Sea. Secondly, we give the theoretical derivation and analysis with combining the normal mode theory with the ray theory. Thirdly, the horizontal-longitudinal correlations at the same receiver depth but in the different high intensity zones are analyzed.

2. Experimental data processing and results

The experiment was conducted in the South China Sea in October 2013 and the experimental setup is the same as that in Ref. [12]. As shown in Fig. 1, the receiving array was a 24-element vertical line array (VLA) deployed at a location with a depth of 143 m–1852 m. The transducer source was towed from Chinese R/V Shi Yan 1 from the Institute of Acoustics, Chinese Academy of Sciences towards the fixed receiving array at a speed of 4 knots. The averaged source depth during the experiment was about 120 m. The linear frequency module (LFM) signals with a duration of 20 s were transmitted twice every 90 s, of which the central frequency was 310 Hz, the band width was 100 Hz and the nominal maximum source level at the transducer resonance was 184.2 dB re 1 μPa @ 1 m as shown in Fig. 2.

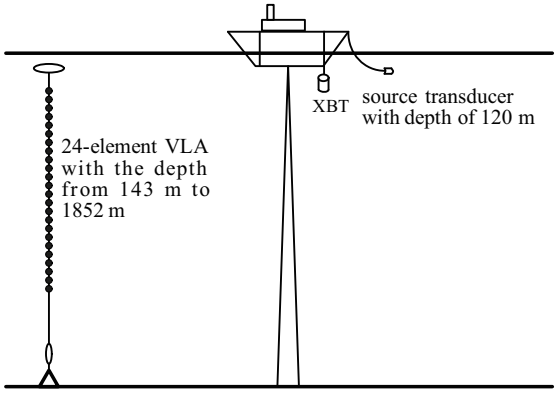


Fig. 1. Experimental configuration.

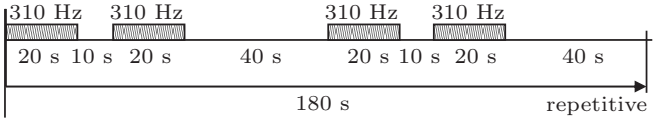


Fig. 2. The time series of the transmitted LFM signals.

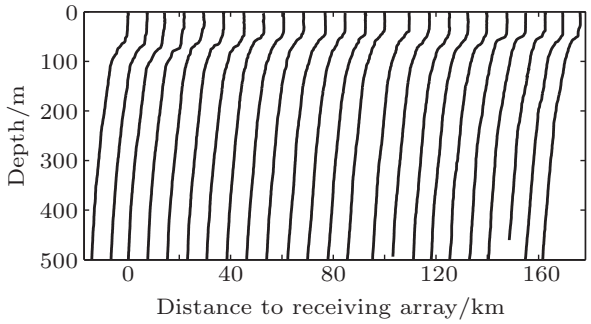


Fig. 3. Temperature profiles measured along the propagation track by XBT.

The temperature profiles along the propagation track were measured using XBT of which the position and the changing trend with depth are shown in Fig. 3. Figure 4 shows the sound speed profiles along the propagation track, which are calculated by the empirical equation in Ref. [13], based on the XBT data. It shows that the sound speed profile is stable and nearly invariable in the experiment. The sound speed profile measured by using CTD casted near the receiving array is shown in Fig. 5. The sound channel axis depth is about 1164 m with a sound speed of 1484.0 m/s. It is a typical incomplete deep sea channel that the surface sound speed is 1540.1 m/s which is greater than that near the bottom 1533 m/s. The maximal propagation range was about 180 km containing three convergence zones. It is nearly a flat bottom with a mean depth of 4305 m along the propagation track. The bottom sediment is core sampled in this experiment, and the results show that the surface bottom density is 1.6 g/cm^3. Reference [14] inverted the bottom acoustic parameters near this experimental area and

the attenuation coefficient was $\alpha = 0.78 f^{2.08}$ dB/m, where the frequency is in units of kHz.

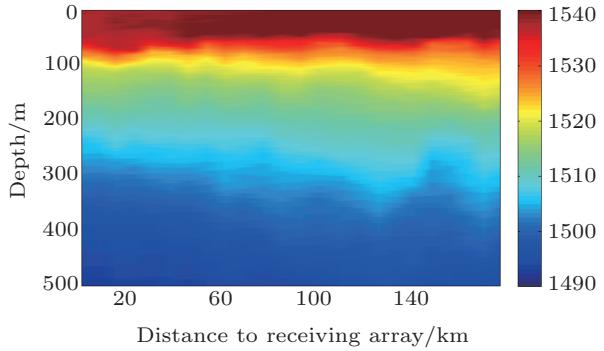


Fig. 4. (color online) Sound speed profiles calculated by XBT data along the propagation track.

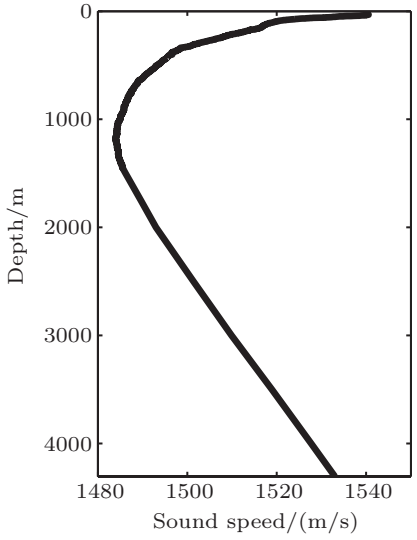


Fig. 5. Sound speed profile measured near the receiving array.

In the signal processing, we first obtain the compressed pulse signal $s_c(t)$ by using the pulse compression technique which can increase the signal-to-noise ratio (SNR). The process is as follows: the original LFM signal from the transducer is denoted as $s(t)$, and the received signal from one element of VLA can be expressed as

$$s_R(t) = \int S(\omega) P(r,z;\omega) \exp(-i\omega t)\, d\omega, \tag{1}$$

where $S(\omega)$ is the spectrum of $s(t)$, and $P(r,z;\omega)$ is the transfer function of the ocean environment from source to receiver. By correlating $s(t)$ with $s_R(t)$, the compressed signal can be expressed as

$$s_c(t) = \int |S(\omega)|^2 P(r,z;\omega) \exp(-i\omega t)\, d\omega. \tag{2}$$

Two receiving signals after pulse compression are shown in Fig. 6. The upper signal is in the first convergence zone with receiver depth 167 m and source–receiver distance 52.56 km and its SNR is about 25.6 dB. The lower signal is in the third shadow zone with receiver depth 1111 m and source–receiver distance 140.61 km and its SNR is about 1.6 dB. It is proved that the SNR of the compressed pulse signals are high enough to calculate the correlation coefficients in the experiment.

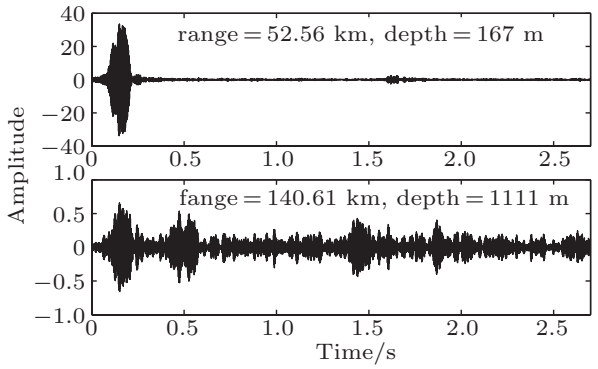


Fig. 6. Two compressed pulse signals.

Then we can obtain the spectrum X_i of $s_c(t)$ based on the FFT method. Finally, we can calculate the average signal energy in the source bandwidth, which can be written as

$$E(f_0) = \frac{2}{f_s * f_s} \frac{1}{nf_2 - nf_1} \sum_{i=nf_1}^{nf_2} |X_i|^2, \tag{3}$$

where f_0 is the central frequency, f_s is the signal sampling rate, nf_1 and nf_2 are the frequency positions of the sampling lower and upper frequencies, respectively. The transmission loss (TL) at a range and depth in the experiment can be expressed as

$$\begin{aligned} &TL(f_0|(r,z)) \\ &= SL(f_0) - (10 * \log_{10}(E(f_0|(r,z))) - M_v - E_c), \end{aligned} \tag{4}$$

where $SL(f_0)$ is the source level of the emitted transducer, M_v is the sensitivity of the receiving hydrophone, and E_c represents the increasing energy of the pulse compression filter. The experimental TL values at different ranges and depths based on Eq. (4) are shown in Fig. 7.

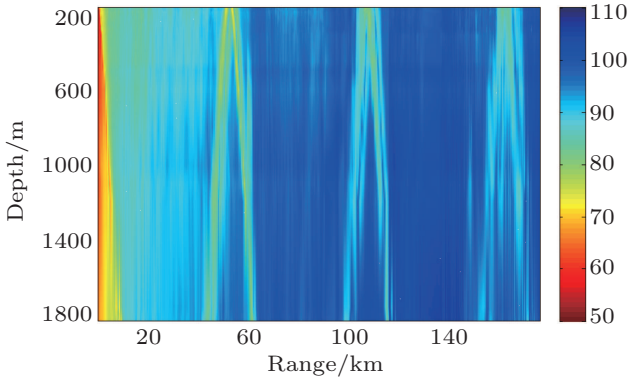


Fig. 7. (color online) Experimental TLs at different ranges and depths. The central frequency of the source is 310 Hz, the band width is 100 Hz, and the source depth is 120 m.

The spatial correlation coefficient is defined as the normalized cross correlation between two spatially separated points' received signals which are from the same source. It

describes the similarity between the waveforms of signals received at two separated points. In practical signal processing, as the received times between two separated points are different, we usually implement time-delay to compensate one signal. The spatial correlation coefficient between positions (r_1, z_1) and (r_2, z_2) can be expressed as

$$\rho(r_1, r_2, z_1, z_2) = \max_{\tau} \frac{\int_{-\infty}^{\infty} p(r_1, z_1, t)\, p(r_2, z_2, t+\tau)\, \mathrm{d}t}{\sqrt{\int_{-\infty}^{\infty} |p(r_1, z_1, t)|^2\, \mathrm{d}t \int_{\omega_1}^{\omega_2} |p(r_2, z_2, t)|^2\, \mathrm{d}t}}, \quad (5)$$

where $p(r_1, z_1, t)$ and $p(r_2, z_2, t)$ are signals received at the two positions, and τ is the time delay. The expression in the frequency domain can be written as

$$\rho(r_1, r_2, z_1, z_2) = \max_{\tau} \frac{\left| \int_{\omega_1}^{\omega_2} p(r_1, z_1, \omega)\, p^*(r_2, z_2, \omega)\, \mathrm{e}^{\mathrm{i}\omega\tau}\, \mathrm{d}\omega \right|}{\sqrt{\int_{\omega_1}^{\omega_2} |p(r_1, z_1, \omega)|^2\, \mathrm{d}\omega \int_{\omega_1}^{\omega_2} |p(r_2, z_2, \omega)|^2\, \mathrm{d}\omega}}, \quad (6)$$

where $p(r_1, z_1, \omega)$ and $p(r_2, z_2, \omega)$ are the spectra of $p(r_1, z_1, t)$ and $p(r_2, z_2, t)$, "$*$" represents complex conjugation, and ω_1 and ω_2 are the lower and upper angular frequencies of the emitted signals, respectively.

Considering the fact that the arrival structure of a deeper received signal is complex and the arrival time length is long, we select the time length of the compressed pulse signals to be 2.7 s to calculate the spatial correlation coefficient. The reference signal is in the first convergence zone where the receiver depth is 167 m and the source–receiver distance is 52.56 km. Let all the received signals at different ranges and depths correlate with the reference signal according to Eq. (5). The experimental spatial correlation coefficients in the whole acoustic field are shown in Fig. 8.

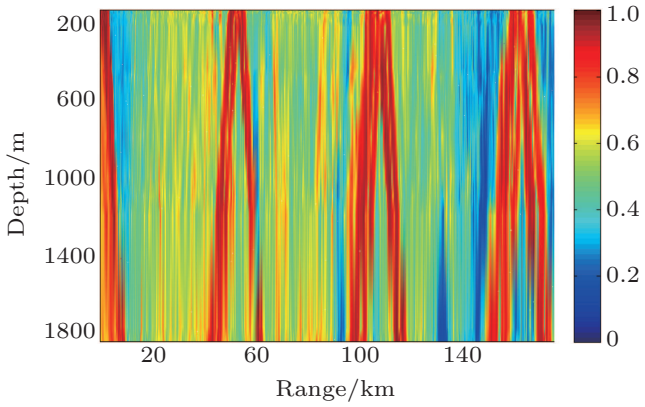


Fig. 8. (color online) Experimental spatial correlation coefficients in the whole acoustic field. The reference signal is in the first convergence zone with the receiver depth of 167 m and source–receiver distance of 52.56 km.

We can conclude that most of the correlation coefficients between the high intensity zones are greater than $\sqrt{2}/2$. But, the correlations between the high intensity zone and the shadow zone are rather low. The structures of the spatial correlation coefficient at different ranges and depths are similar to the transmission loss structure as shown in Fig. 7.

3. Simulated results and theoretical analysis

For comparison with the experimental results, we use the normal mode program KrakenC to calculate the acoustic field. Although the source is moving and the receiving array is fixed in the experiment, we can use the reciprocity principle to simulate the sound field because the bottom is flat and the sound speed profile along the propagation track is stable as shown in Fig. 4. In the simulation, we use the single sound speed profile in Fig. 5. The seafloor acoustic parameters are based on the matching of the experimental TL in the shadow zone. The two-layer liquid bottom model is used and the thickness of the sediment layer is 5 m. The sound speed is 1565 m/s, the density is 1.6 g/cm^3, and the attenuation coefficient is 0.09 dB/m inside the sediment layer. The infinite basement has a sound speed of 1650 m/s, a density of 1.8 g/cm^3, and an attenuation coefficient of 0.14 dB/m. Figure 9 shows the simulated TLs at different ranges and depths and the comparison between the simulated and experimental TLs at receiver depth 167 m. It can be seen that the simulated TLs are in good agreement with the experimental TLs.

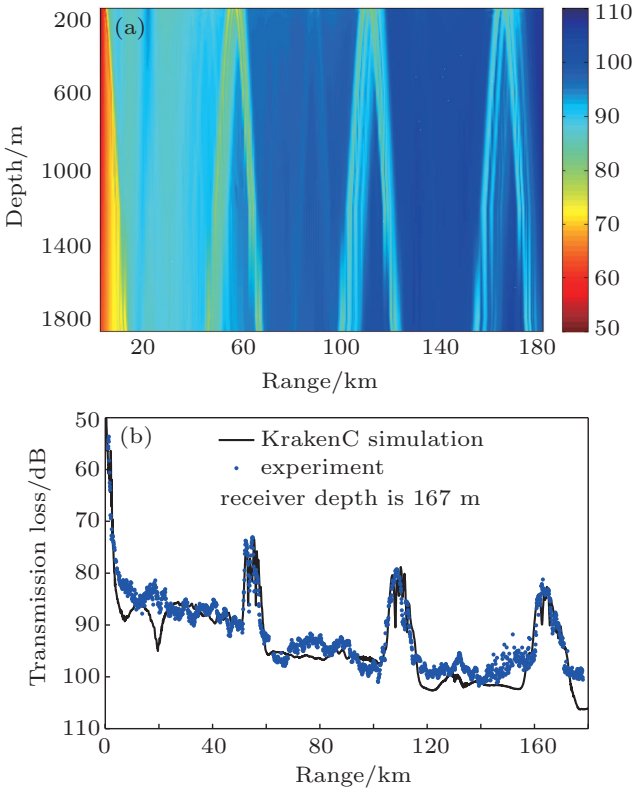


Fig. 9. (color online) Simulated TLs at different ranges and depths (a). Comparison between KrakenC simulated and experimental TLs at receiver depth 167 m (b).

The simulated spatial correlation coefficient is obtained by substituting the simulated pressure into Eq. (6). Figure 10 shows the spatial distribution of the simulated spatial correlation coefficients in the whole acoustic field where the reference pressure position is the same as that in Fig. 8. It can be seen from Figs. 8 and 10 that the spatial distribution of the simulated spatial correlations in the whole acoustic field is consistent with the experimental results. They all show that the correlation coefficients between the high intensity zones are high, but they are low between the high intensity zone and the shadow zone.

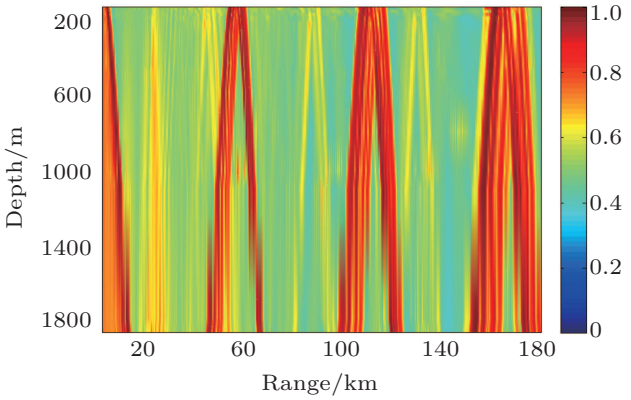


Fig. 10. (color online) Simulated spatial correlation coefficients in the whole acoustic field. The reference pressure position is the same as that in Fig. 8.

To explain qualitatively why the correlation coefficients between high intensity zones are high, we analyze the modes and arrival times of the simulated signals in the high intensity zone by combining the normal mode theory with the ray theory. Figure 11 shows the phases of the first 600 modes of the simulated reference pressure where the source depth is 120 m, the receiver depth is 167 m and the source–receiver distance is 52.56 km. Figure 12 shows the main ray tracks, arrival times and relative amplitudes by the ray program Bellhop of the simulated reference pressure. It can be seen from Fig. 11 that the first group of modes consist of modes 200–210 whose phases are close. The corresponding group speeds of these modes at a frequency 310 Hz are in a range of about 1487.6 m/s–1488.1 m/s and the phase speeds are 1515.4 m/s–1516.8 m/s. The phase speed is close to the seawater sound speed at a depth of 167 m, which is 1515.2 m/s–1515.5 m/s. We can calculate the arrival times by dividing the source–receiver distance by group speed to be about 35.32 s–35.33 s, which correspond to the refraction path rays (the red lines) in Fig. 12(a) and the amplitudes are highest as shown in Fig. 12(b). The second group of modes which have close phases are near mode 334, of which the group speed is 1487.1 m/s and the calculated arrival time is about 35.34 s. The phase speed is 1533.7 m/s which is close to the bottom sound speed, so these modes correspond to those that go through once bottom reflection (BR) rays (the blue lines) as shown in Fig. 12(a) and the relative amplitudes are low as shown in Fig. 12(b). In the same way, the third group of modes correspond to those that go through twice BRs and once surface reflection (SR) or twice BRs and twice SRs rays(the black lines) in Fig. 12(a). The group speed of mode 560 is about 1429.5 m/s, and the arrival time is about 36.8 s. The relative amplitudes of the third group of modes are rather small, as shown in Fig. 12(b). We can find that the energy of simulated pressure is mainly contributed from the first group of modes. The ray tracks and the main modes of the acoustic field in all high intensity zones have the same characteristics as those shown in Figs. 11 and 12.

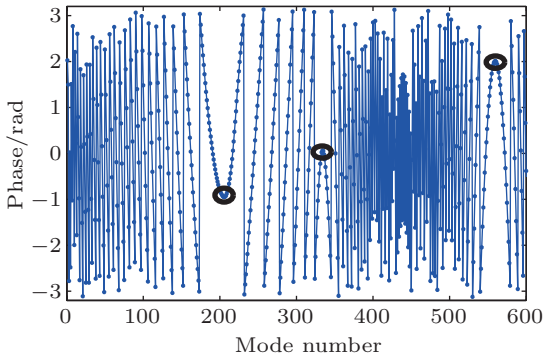


Fig. 11. (color online) Phases of the first 600 modes of the simulated reference pressure. The frequency is 310 Hz.

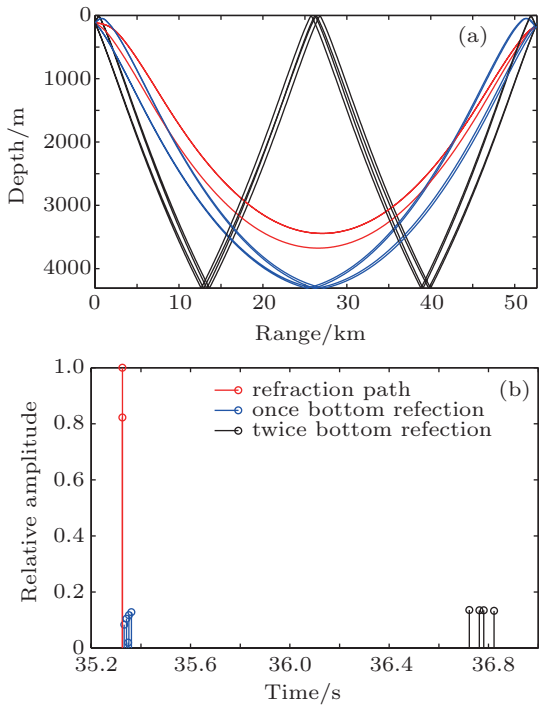


Fig. 12. (color online) (a) Plots of depth versus range, and (b) relative amplitudes versus time for different arrival paths, obtained by the ray program Bellhop of the simulated reference pressure.

To better understand this phenomenon, we give the theoretical analysis in the following. On condition that the ocean environmental parameters depend only on depth, the underwater acoustic pressure field generated by a harmonic point

source derived from the normal mode theory is[15]

$$p(\omega,r,z) = \frac{1}{\rho(z_s)\sqrt{8\pi r}}\sum_{l=1}^{\infty}\psi_l(\omega,z_s)\psi_l(\omega,z)\frac{e^{i\mu_l r-\beta_l r+i\pi/4}}{\sqrt{\mu_l(\omega)}}, \quad (7)$$

where z_s and z are the source and receiver depths, ψ_l is the eigenfunction of the l-th normal mode, and μ_l and β_l are the real and imaginary parts of the eigenvalue of the l-th mode, β_l is also called the attenuation coefficient because it is due to the boundary loss and volume absorption.

In Eq. (6), the denominator is the normalization factor of the spatial correlation coefficient. By substituting the sound pressure in Eq. (7) into Eq. (6), the cross term in the integral in the numerator can be written as

$$\begin{aligned}&\int_{\omega_1}^{\omega_2} p(r_1,z_1,\omega)p^*(r_2,z_2,\omega)e^{i\omega\tau}d\omega\\ &= \int_{\omega_1}^{\omega_2}\frac{e^{i\omega\tau}}{\rho^2(z_s)8\pi\sqrt{r_1r_2}}\sum_l\psi_l^2(z_s)\psi_l(z_1)\psi_l(z_2)\\ &\quad\times\frac{e^{-\beta_l(r_1+r_2)-i\mu_l\Delta r}}{\mu_l}d\omega\\ &\quad+\int_{\omega_1}^{\omega_2}\frac{e^{i\omega\tau}}{\rho^2(z_s)8\pi\sqrt{r_1r_2}}\sum_{l\neq m}\sum_m\psi_l(z_s)\psi_m(z_s)\psi_l(z_1)\psi_m(z_2)\\ &\quad\times\frac{e^{i(\mu_l-\mu_m)r_1-(\beta_l r_1+\beta_m r_2)-i\mu_m\Delta r}}{\sqrt{\mu_l\mu_m}}d\omega, \quad (8)\end{aligned}$$

where $\Delta r = r_2 - r_1$. Generally, there are many modes transmitting in a deep ocean sound channel. The first term on the right-hand side of Eq. (8) in the high intensity zone is a slowly varying function of ω due to the strong correlation between the same modes. However, the second term in the integral varies rapidly with depth and range because of the weak correlation between different modes and vanishes when it is integrated in the frequency bandwidth. So equation (8) can be simplified into

$$\begin{aligned}&\int_{\omega_1}^{\omega_2} p(r_1,z_1,\omega)p^*(r_2,z_2,\omega)e^{i\omega\tau}d\omega\\ &\approx\int_{\omega_1}^{\omega_2}\frac{e^{i\omega\tau}}{\rho^2(z_s)8\pi\sqrt{r_1r_2}}\sum_l\psi_l^2(z_s)\psi_l(z_1)\psi_l(z_2)\\ &\quad\times\frac{e^{-\beta_l(r_1+r_2)-i\mu_l\Delta r}}{\mu_l}d\omega. \quad (9)\end{aligned}$$

The characteristics of the signal pulses in the high intensity zones are that the main pulses arrive first, the corresponding group speeds of the modes are nearly identical and the phases vary slowly. So the modes which contribute the main energy are nearly of coherent superposition.[16] In the calculation, we can ignore the later arrival pulses, of which the amplitudes are small and the energies are low. Assume that the in-phase modes of the main pulses in high intensity zones are $m \to n$, they satisfy $\mu_m \approx \mu_{m+1} \approx \cdots \approx \mu_n$, equation (9) can be written as

$$\begin{aligned}&\int_{\omega_1}^{\omega_2} p(r_1,z_1,\omega)p^*(r_2,z_2,\omega)e^{i\omega\tau}d\omega\\ &\approx\int_{\omega_1}^{\omega_2} e^{i\omega\tau}\sum_{l=m\to n}A_l(\omega,\Delta r,z_1,z_2)e^{-i\mu_l\Delta r}d\omega, \quad (10)\end{aligned}$$

where $A_l(\omega,\Delta r,z_1,z_2)$ can be expressed as

$$A_l(\omega,\Delta r,z_1,z_2) = \frac{1}{\rho^2(z_s)8\pi\sqrt{r_1r_2}}\psi_l^2(z_s)\psi_l(z_1)\psi_l(z_2)\frac{e^{-\beta_l(r_1+r_2)}}{\mu_l}. \quad (11)$$

By substituting Eq. (10) into Eq. (6), the spatial correlation coefficient in the high intensity zone of the deep water acoustic field can be expressed as

$$\rho(r_1,r_2,z_1,z_2) \approx \max_\tau \frac{\left|\int_{\omega_1}^{\omega_2}\sum_{l=m\to n}\psi_l^2(\omega,z_s)\psi_l(\omega,z_1)\psi_l(\omega,z_2)e^{-\beta_l(r_1+r_2)}e^{i(\mu_m-\mu_l)\Delta r}e^{i\omega\tau}d\omega\right|}{\sqrt{\int_{\omega_1}^{\omega_2}\left|\sum_{l=1}^{\infty}\psi_l(\omega,z_s)\psi_l(\omega,z_1)e^{-\beta_l r_1}e^{i\mu_l r_1}\right|^2 d\omega\int_{\omega_1}^{\omega_2}\left|\sum_{l=1}^{\infty}\psi_l(\omega,z_s)\psi_l(\omega,z_2)e^{-\beta_l r_2}e^{i\mu_l r_2}\right|^2 d\omega}}. \quad (12)$$

It has been widely shown that the correlation is degraded by scattering and multipath interference. Decorrelation by scattering may be caused by temperature fluctuations, surface waves, bottom roughness or internal waves. However, from Eq. (12) we know that the spatial correlations of the high intensity zone are mainly affected by the phases of main modes. The simulated results show that the received signals in the high intensity zone are all mainly contributed from the first in-phase waterborne mode group. As indicated in Ref. [9], the received signals in high intensity zones have the same waveform as an emitted signal or its Hilbert transform. So most of the correlation coefficients between the high intensity zones are mostly high.

4. Horizontal–longitudinal correlation in high intensity zones

What is more, the horizontal–longitudinal correlations at the same receiver depth but in different high intensity zones are analyzed. Firstly, we select the horizontal–longitudinal correlations in the three high intensity zones at the receiver

depth of 167 m from Figs. 5 and 7. The reference signal is in the first convergence zone with a source–receiver distance of 52.56 km. Figure 13 shows the comparisons between the simulated and experimental results. Figure 14 displays the experimental waveforms of the compressed pulse reference signal and four signals (where the source–receiver distances are 164.6 km, 55.2 km, 55.3 km, and 165.7 km, respectively.). The horizontal–longitudinal correlation coefficients between the reference signal and the four signals are 0.93, 0.83, 0.72, and 0.63, respectively. We can find that the horizontal–longitudinal correlation coefficients between the different high intensity zones are also high at a receiver depth of 167 m and the received signals are mainly contributed from one pulse. But, the main pulse encounters two parts at some positions, and the correlation coefficient becomes smaller with the two parts appearing more obvious.

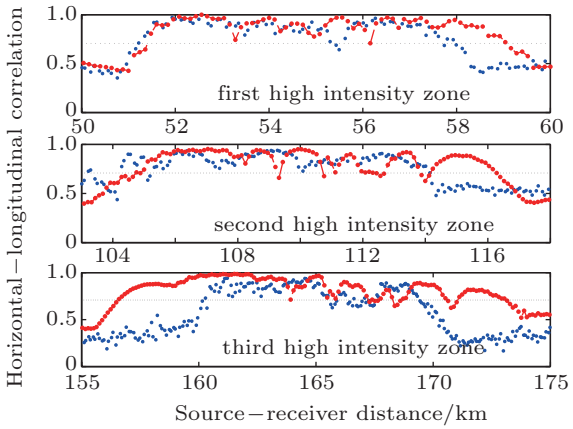


Fig. 13. (color online) Comparisons between simulated (red dotted curves) and experimental (blue dotted curves) horizontal–longitudinal correlation coefficients in three convergence zones where the receiver depth is 167 m. The source–receiver distance of the reference signal is 52.56 km.

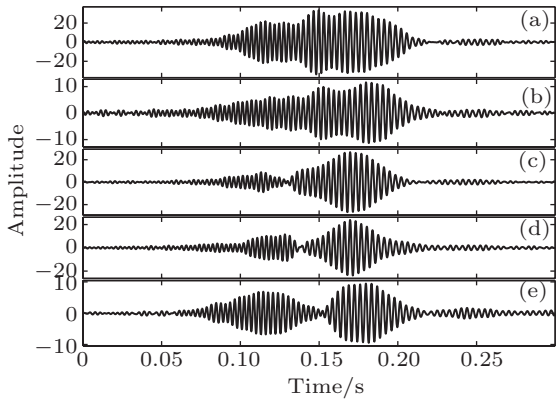


Fig. 14. The waveforms of the experimental signals at receiver depth 167 m, where the source–receiver distances are (a) 52.56 km (the reference signal), (b) 164.6 km (the correlation is 0.93), (c) 55.2 km (the correlation is 0.83), (d) 55.3 km (the correlation is 0.72), and (e) 165.7 km (the correlation is 0.64).

Similarly, the comparisons between the simulated and experimental horizontal–longitudinal correlations in the three high intensity zones at the receiver depth of 1111 m where the reference signal is in the first convergence zone with a source–receiver distance of 59.6 km are shown in Fig. 15. Figure 16 displays the experimental waveforms of the compressed pulse reference signal and four signals (where the source–receiver distances are 47.2 km, 48.9 km, 51.0 km, and 49.4 km, respectively). The horizontal–longitudinal correlation coefficients between the reference signal and the four signals are 0.92, 0.84, 0.74, and 0.47. We can find that the received signals where the horizontal–longitudinal correlation coefficient is high at depth 1111 m are mainly contributed from one pulse, the same as that with the signals at depth 167 m. However, when the correlation coefficient becomes low, the multi-path arrival structure of the corresponding received signal at depth 1111 m is more complex than that at 167 m.

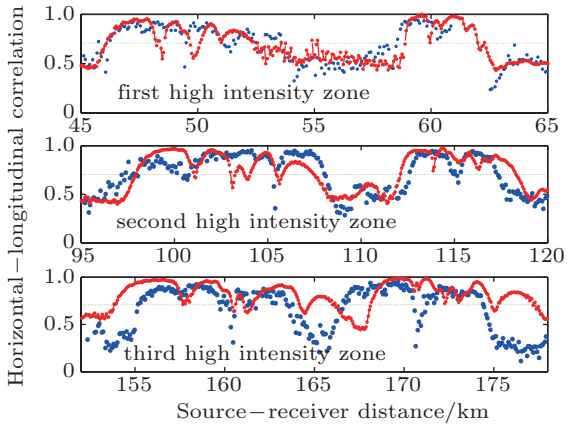


Fig. 15. (color online) Comparisons between simulated (red dotted curves) and experimental (blue dotted curves) longitudinal–correlation coefficients in the high intensity zones where the receiver depth is 1111 m and the source–receiver distance of the reference signal is 59.6 km.

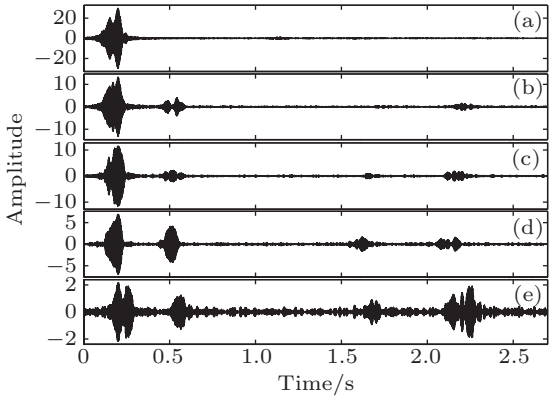


Fig. 16. Waveforms of the experiment signals at different ranges, where the receiver depth is 1111 m and the receiver ranges are (a) 59.6 km (the reference signal), (b) 47.2 km (the correlation is 0.92), (c) 48.9 km (the correlation is 0.84), (d) 51.0 km (the correlation is 0.74), (e) 49.4 km (the correlation is 0.47).

We analyze the multi-path arrival structure of the signal where the source–receiver distance is 49.4 km as shown in Fig. 16(e). Its ray tracks, arrival times and amplitudes by the ray program Bellhop of the corresponding simulated pressure are shown in Fig. 17. It proves that the first pulse is mainly formed from the refraction path rays (red lines) and happens

to go through BR path rays once (blue lines) as shown in Fig. 17(a). The second pulse is mainly from the pulses that go through once BR and once SR rays (black lines). The third pulse is formed from the pulses that go through BRs twice and SR rays once (green lines), and the fourth pulse corresponds to the red dash lines which go through BRs and SRs twice. The correlation coefficient will be 0.72 if the first 0.4 s of Fig. 16(e) is correlated with the reference signal. It shows that the structure of the first arrival signal in the high intensity zone is composed of the refraction path rays and the contributed modes are unanimous. At some positions, more pulses are received in the arrival structure of the signal due to bottom reflection, and the horizontal–longitudinal correlation coefficient decreases accordingly.

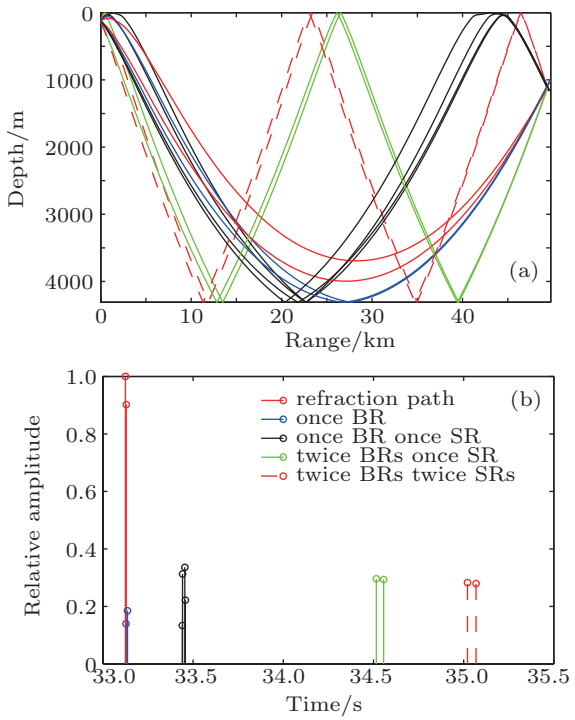


Fig. 17. (color online) Plots of depth versus range (a) and relative amplitude versus times (b) for different paths, obtained by the ray program Bellhop, where the receiver depth is 1111 m and range is 49.4 km.

5. Conclusions and perspectives

The spatial correlations of the high intensity zone in the deep water acoustic field are investigated by using the experimental data obtained in the South China Sea and analyzed by combining the normal modes theory with the ray theory. It is shown that most of the correlation coefficients between the high intensity zones are greater than $\sqrt{2}/2$. But, the correlations between the high intensity zone and the shadow zone are rather low. The structures of the spatial correlation coefficient at different ranges and depths are similar to the transmission loss structure in deep water. The received signals in the high intensity zone mainly include one or two main pulses which are contributed by the interference of a group of waterborne modes with similar phases. The main pulses in different high intensity zones are also contributed from the same modes.

What is more, the horizontal–longitudinal correlations at the same receiver depth but in the different high intensity zones are analyzed. The horizontal–longitudinal correlations are high in general. However, at some positions, more pulses are received in the arrival structure of the signal due to bottom reflection and the horizontal–longitudinal correlation coefficient decreases accordingly. The multi-path arrival structure of the receiving signal becomes more complex and the corresponding influence of the bottom reflection rays becomes greater with increasing receiver depth.

Acknowledgment

The authors thank all the researchers for their help in the experiment in 2013. This work was supported by the Joint NSFC–ISF Research Program, jointly funded by the National Natural Science Foundation of China and the Israel Science Foundation.

References

[1] Urick R J 1973 *J. Acoust. Soc. Am.* **54** 115
[2] Zhou S H, Zhang R H, Tao X D, *et al.* 1998 *Progress in Natural Science* **8** 342 (in Chinese)
[3] Chen Y, Ni M and Zhang Z H 2011 *Appl. Acoust.* **30** 295 (in Chinese)
[4] Wang Y, Gong Z X and Lin P 2016 *Sci. Sin.-Phys. Mech. Astron* **46** 090000 (in Chinese)
[5] Hale F E 1961 *J. Acoust. Soc. Am.* **33** 456
[6] Urick R J and Lund G R 1968 *J. Acoust. Soc. Am.* **43** 723
[7] Urick R J 1965 *J. Acoust. Soc. Am.* **38** 348
[8] Zhang R H 1980 *Acta Acustica* **5** 28 (in Chinese)
[9] Zhang R H 1982 *Acta Acustica* **7** 75 (in Chinese)
[10] Gorodetskaya E Y, Malekhanov A I, Sazontov A G, *et al.* 1999 *IEEE J. Oceanic Engineering* **24** 156
[11] John A C and Tarun K C 2013 *J. Acoust. Soc. Am.* **134** 3119
[12] Li J, Li Z L, Ren Y, Li W and Zhang R H 2015 *Chin. Phys. Lett.* **32** 064303
[13] Mackenzie K V 1981 *J. Acoust. Soc. Am.* **70** 807
[14] Wu S L, Li Z L and Qin J X 2015 *Chin. Phys. Lett.* **32** 124301
[15] Jensen F B, Kuperman W A, Porter M B and Schmidt H 2011 *Computational Ocean Acoustics*, 2nd edn. (New York: Springer) p. 340
[16] Chen L R 2014 "Matched field source localization in deep water using Gaussian Beam method", Ph. D. Dissertation (Beijing: Institute of Acoustics, Chinese Academy of Sciences) (in Chinese)